

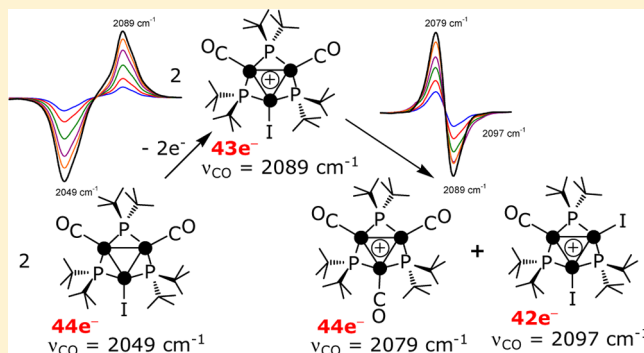
Synthesis and Spectroscopic and Spectroelectrochemical Characterization of a New Family of 44e[−] Tris-Phosphido-Bridged Palladium Triangles

Veronica Bonuccelli, Tiziana Funaioli, Piero Leoni,* Fabio Marchetti, and Lorella Marchetti

Dipartimento di Chimica e Chimica Industriale dell'Università di Pisa, Via Risorgimento 35, I-56126 Pisa, Italy

S Supporting Information

ABSTRACT: Triangular clusters containing a $[M_3(\mu\text{-PR}_2)_3]^+$ core are very common in platinum chemistry but were virtually unknown for $M = \text{Pd}$. Herein we describe the synthesis and characterization of several palladium derivatives belonging to this class. The trinuclear monohalide clusters $\{\text{Pd}_3\}(\text{CO})_2\text{X}$ [$\{\text{Pd}_3\} = \text{Pd}_3(\mu\text{-P}^t\text{Bu}_2)_3$; $\text{X} = \text{Br}, \text{I}$] were prepared by reacting $[\text{Bu}_4\text{N}]\text{X}$ or KX with the dinuclear complex $[\text{Pd}(\text{P}^t\text{Bu}_2\text{H})(\mu\text{-P}^t\text{Bu}_2)_2]$ and H_2O under an atmosphere of CO . The reaction of $\{\text{Pd}_3\}(\text{CO})_2\text{I}$ with CNBu^t leads to the substitution of all the terminal ligands to afford the symmetrical cluster $[\{\text{Pd}_3\}(\text{CNBu}^t)_3]\text{I}$. The latter reacts with TIPF_6 (excess) or AgCF_3SO_3 (1:1 ratio) to give anion metathesis, whereas the addition of a second equivalent of Ag^+ causes cluster oxidation to the thermally stable paramagnetic $43e^-$ dication $[\{\text{Pd}_3\}(\text{CNBu}^t)_3]^{2+}$. The cationic clusters $[\{\text{Pd}_3\}(\text{CO})_2(\text{L})]\text{PF}_6$ ($\text{L} = \text{NCCH}_3, \text{Py}$ or CO) were obtained by reacting $\{\text{Pd}_3\}(\text{CO})_2\text{I}$ with TIPF_6 under nitrogen in acetonitrile or in pyridine or under 1 atm of carbon monoxide in THF. Finally, $\{\text{Pd}_3\}(\text{CO})_2\text{Cl}$ was achieved by the reaction of $[\{\text{Pd}_3\}(\text{CO})_3]\text{PF}_6$ with $[(\text{PPh}_3)_2\text{N}]\text{Cl}$. All clusters have been obtained in good yields and purity and have been characterized by microanalysis and IR and multinuclear NMR spectroscopy. Single crystal X-ray diffraction studies on $\{\text{Pd}_3\}(\text{CO})_2\text{Br}$ and $[\{\text{Pd}_3\}(\text{CNBu}^t)_3]\text{CF}_3\text{SO}_3$ are also reported. The cyclovoltammetric profile exhibited by the palladium clusters prepared in this work is characterized by the presence of two monoelectronic oxidation processes whose reversibility and potentials depend on the nature of the ligands. Moreover, the UV–vis and IR spectroelectrochemical analysis of $\{\text{Pd}_3\}(\text{CO})_2\text{I}$, $[\{\text{Pd}_3\}(\text{CO})_3]\text{PF}_6$ and $[\{\text{Pd}_3\}(\text{CNBu}^t)_3]\text{PF}_6$ allowed the spectroscopical characterization of some electrogenerated oxidized species and provided some detail for the redox-coupled reactions of metastable products.



1. INTRODUCTION

Tris-phosphido-bridged clusters of platinum are well-known.^{1–4} They have a common $[\text{Pt}_3(\mu\text{-PR}_2)_3]^+$ moiety, with a triangular mixed-valence (Pt_3^{4+}) metal core; the structures are completed by three terminal ligands in the cationic clusters $[\text{Pt}_3(\mu\text{-PR}_2)_3(\text{L})_3]^+$ ($\text{L} = \text{CO}, \text{PR}_3, \text{RNC}, \text{RCN}, \text{C}_2\text{H}_4$, or mixtures of them) or in the neutral derivatives $\text{Pt}_3(\mu\text{-PR}_2)_3(\text{L})_2\text{X}$ ($\text{L} = \text{CO}, \text{PR}_3, \text{RNC}$; $\text{X} = \text{H}, \text{Ar}, \text{Cl}, \text{Br}, \text{I}, \text{CCR}, \text{SiR}_3$).^{1,2} Many of them have been prepared in our laboratories,² and we have then shown how they can be employed as precursors of dibridged-tetrahedral hexanuclear clusters³ or polycluster structures,⁴ in which two or more cluster units can be inserted into ordered molecular assemblies by connecting them with strongly bound alkynyl spacers. In attempting to extend this chemistry to the analogous palladium derivatives, we found a unique example of mixed-valence tris-phosphido-bridged triangle cluster of palladium, namely, the chloro derivative $\text{Pd}_3(\mu\text{-P}^t\text{Bu}_2)_3(\text{CO})_2\text{Cl}$ which, however, was obtained in very low yields (12%) as a byproduct in a reaction conceived for other purposes.⁵ Other less related derivatives reported up to now feature a Pd_3^{6+} core, as found in the bis(dialkylamino)phosphide derivatives $\text{Pd}_3(\mu\text{-}$

$\text{PR}_2)_3\text{Cl}_3$ [$\text{R} = \text{NPr}^i_2, \text{N}(c\text{-Hex})_2$],⁶ and in the primary phosphido derivative,⁷ $\text{Pd}_3(\mu\text{-PHCH}_2\text{Fc})_3(\text{PPh}_3)_3\text{Cl}_3$, or contain bridging phosphine ligands, as found in the $42e^-$ cluster $\text{Pd}_3(\mu\text{-PC}_5\text{H}_2\text{-2,4,6-Ph}_3)_3(\text{PEt}_3)_3$.⁸ Herein we describe high yield synthetic procedures for the neutral clusters $\{\text{Pd}_3\}(\text{CO})_2\text{X}$ [$\{\text{Pd}_3\} = \text{Pd}_3(\mu\text{-P}^t\text{Bu}_2)_3$; $\text{X} = \text{Cl}, \text{Br}, \text{I}$] and for $[\{\text{Pd}_3\}(\text{L})_2\text{L}']\text{X}$ ($\text{L} = \text{CO}, \text{L}' = \text{CO}, \text{MeCN}, \text{Py}$, $\text{X} = \text{PF}_6$; and $\text{L} = \text{L}' = \text{CNBu}^t$, $\text{X} = \text{I}, \text{PF}_6, \text{CF}_3\text{SO}_3$). The new clusters were characterized by microanalytical and spectroscopical (IR and ^1H , ^{13}C , and ^{31}P NMR) analyses and by cyclovoltammetric and spectroelectrochemical studies. Single crystal X-ray diffraction studies on the structures of $\{\text{Pd}_3\}(\text{CO})_2\text{Br}$ and $[\{\text{Pd}_3\}(\text{CNBu}^t)_3]\text{CF}_3\text{SO}_3$ are also described.

2. RESULTS AND DISCUSSION

2.1. Syntheses. The neutral monohalide clusters $\{\text{Pd}_3\}(\text{CO})_2\text{X}$ [2, $\text{X} = \text{Br}$; 3, $\text{X} = \text{I}$] were obtained by adding the

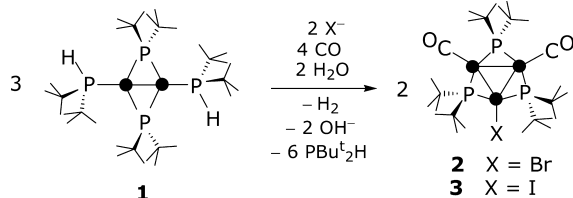
Received: April 16, 2013

Published: July 24, 2013



corresponding potassium or *n*-butylammonium halide and a molar excess of water to a toluene suspension of the dinuclear Pd(I) complex $[\text{Pd}(\text{P}^t\text{Bu}_2\text{H})(\mu\text{-P}^t\text{Bu}_2)_2]_2$ (**1**).⁹ After stirring for three days at 100 °C under 1 atm of carbon monoxide, the final basic mixture was shown by ³¹P NMR to contain the free secondary phosphine, $\text{P}^t\text{Bu}_2\text{H}$, and **2** or **3** in ca. 3:1 ratio; moreover, the evolution of dihydrogen in the course of the reaction was verified by GC analysis (see Experimental Section). We have no clarifying experimental evidence about the mechanism of these probably complex reactions, although, based on the observed formation of $\text{P}^t\text{Bu}_2\text{H}$, H_2 , and OH^- as coproducts of the reactions, the precise stoichiometric balance shown in Scheme 1 can be given. The final products were

Scheme 1. Synthesis of $\{\text{Pd}_3\}(\text{CO})_2\text{X}$ (X = Br, I)

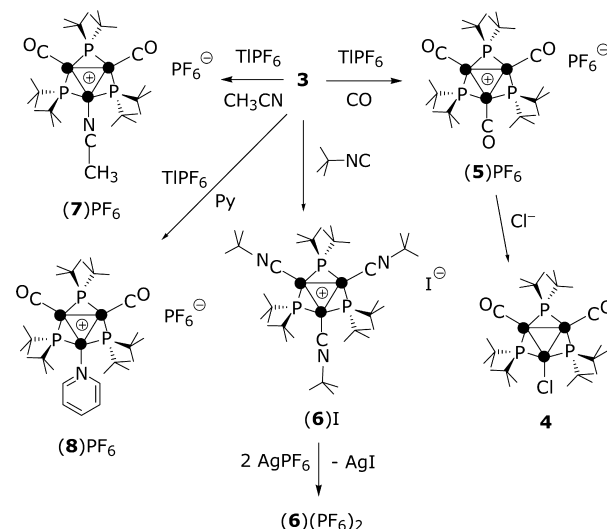


obtained analytically pure in satisfactory to good yields (**2**, 63%; **3**, 85%) as dark red microcrystalline solids soluble in polar and nonpolar organic solvents. In contrast, the synthesis of the chloro derivative $\{\text{Pd}_3\}(\text{CO})_2\text{Cl}$ (**4**), attempted by reacting **1** and $[\text{Bu}_4\text{N}]\text{Cl}$ under analogous conditions, was unsuccessful and gave only complex mixtures of unidentified products. This failure must be assigned to the instability of an intermediate, since **4** was successfully prepared in high yield by an alternative route (vide infra).

Cluster **3** is air stable both in the solid state and in solution, whereas **2** is air stable only in the solid state and decomposes in solution after a few days, giving a mixture of unidentified compounds; both compounds are stable under nitrogen. As confirmed by a crystallographic study (see below), the clusters contain six bulky *tert*-butyl substituents which hinder and stabilize the central Pd_3P_3 core, leaving only three reactive positions available for the functionalization of the cluster, i.e., those occupied by the terminal ligands, which are localized on the Pd_3P_3 plane and mutually directed at 120°. Analogous features were observed in the parent platinum derivatives $\text{Pt}_3(\mu\text{-P}^t\text{Bu}_2)_3(\text{CO})_2\text{X}$, and make them suitable synthons for the synthesis of large molecular frameworks.^{4a,b}

Compound **3** proved to be an excellent precursor for other trinuclear palladium clusters. The reaction of **3** with the isocyanide donor CNBu^t (Scheme 2) leads to the substitution of all the terminal ligands and affords the symmetrical cationic cluster $[\text{Pd}_3(\mu\text{-P}^t\text{Bu}_2)_3(\text{CNBu}^t)_3]\text{I}$, (**6**)**I**, which was isolated as an orange solid in good yield (87%, Scheme 2). The iodide anion, which complicates the cyclic voltammetric profile of the cation (vide infra), was exchanged by treating (**6**)**I** with an excess of TIPF_6 or with a stoichiometric amount of AgCF_3SO_3 . The metathesis reactions afford in quantitative yields (**6**) PF_6 or (**6**) CF_3SO_3 , respectively. The paramagnetic dicationic product (**6**) PF_6 ₂ was isolated in nearly quantitative yield as a dark pink solid after addition of a 2-fold excess of AgPF_6 to a dry CH_2Cl_2 solution of (**6**)**I**. Under ambient atmosphere, (**6**) PF_6 ₂ decomposes in few hours both in the solid state and in CH_2Cl_2 solution, whereas it is relatively stable under inert

Scheme 2. Reactions of Cluster 3



atmosphere (unchanged after 6 days in the solid state, $\tau_{1/2}$ ca. 10 days in solution).

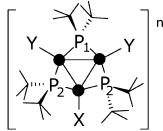
The stepwise substitution of the terminal ligands of cluster **3**, yielding $[\text{Pd}_3(\mu\text{-P}^t\text{Bu}_2)_3(\text{CO})_2(\text{CNBu}^t)]\text{I}$ or $\text{Pd}_3(\mu\text{-P}^t\text{Bu}_2)_3(\text{CNBu}^t)_2\text{I}$, was attempted by reacting the cluster with an equimolar amount or a 2-fold excess of CNBu^t , but in all cases we isolated only mixtures of the starting material **3** and of the persubstituted cluster (**6**)**I**. Conversely, the iodo ligand may be cleanly and quantitatively removed by reacting cluster **3** with an excess of TIPF_6 in acetonitrile or in pyridine. These reactions afford $[\text{Pd}_3(\mu\text{-P}^t\text{Bu}_2)_3(\text{CO})_2(\text{NCCH}_3)]\text{PF}_6$, (**7**) PF_6 (86%), or $[\text{Pd}_3(\mu\text{-P}^t\text{Bu}_2)_3(\text{CO})_2(\text{Py})]\text{PF}_6$, (**8**) PF_6 (74%), respectively, as dark red solids.

Moreover, by treating a dry THF solution of **3** with TIPF_6 under 1 atm of carbon monoxide, the symmetrical cationic cluster $[\text{Pd}_3(\mu\text{-P}^t\text{Bu}_2)_3(\text{CO})_3]\text{PF}_6$, (**5**) PF_6 (77%), was obtained as a red solid. The latter was employed as the precursor of the previously mentioned cluster **4**, which was obtained by adding an equimolar amount of $[(\text{PPh}_3)_2\text{N}]\text{Cl}$ to a solution of (**5**) PF_6 in dry acetone.

Significant IR and NMR parameters for clusters **2**–**8**⁺ are shown in Table 1. The IR ν_{CO} absorptions of the neutral monohalides **2**–**4** were found at ca. 2030–2040 cm^{-1} , which, in comparison to the corresponding bands of cation **5**⁺ (ν_{CO} = 2094, 2053 cm^{-1}), are shifted as expected for the substitution of a π -acceptor carbonyl with a σ -donor halide ligand and for the resulting charge reduction. Cations **7**⁺ and **8**⁺, containing a σ -donor nitrogen ligand, show ν_{CO} absorptions at intermediate frequencies (2044–2066 cm^{-1}). The isocyanide derivative **6**⁺ shows the ν_{CN} absorption at 2156 cm^{-1} , higher than in free CNBu^t (2136 cm^{-1}); similar frequencies were found in other trinuclear palladium clusters with terminal isocyanide ligands (ν_{CN} = 2175 and 2148 cm^{-1} in $[\text{Pd}_3(\mu\text{-SO}_2)_2(\text{CNBu}^t)_2(\text{PBz}_3)_3]^{10}$ and 2138 cm^{-1} in $[\text{Pd}_3(\mu\text{-P}^t\text{Bu}_2)_2(\text{CN-C}_6\text{H}_4\text{-}p\text{-Me})_3](\text{CF}_3\text{SO}_3)_2]^{11}$).

The IR spectra of (**6**) PF_6 ₂ show the expected shift of the ν_{CN} absorption (2193 cm^{-1} , solid state) compared to the monocationic (**6**)**I**. Identical data were found for the dication **6**²⁺ obtained after electrolysis during the IR spectroelectrochemical experiments (see below). Due to the paramagnetism of (**6**) PF_6 ₂, its ³¹P{¹H} NMR spectrum does not

Table 1. Significant IR ν [cm^{-1} , Solid State (CH_2Cl_2 Solution)] and NMR δ [ppm] Parameters for Clusters 2–(8) PF_6

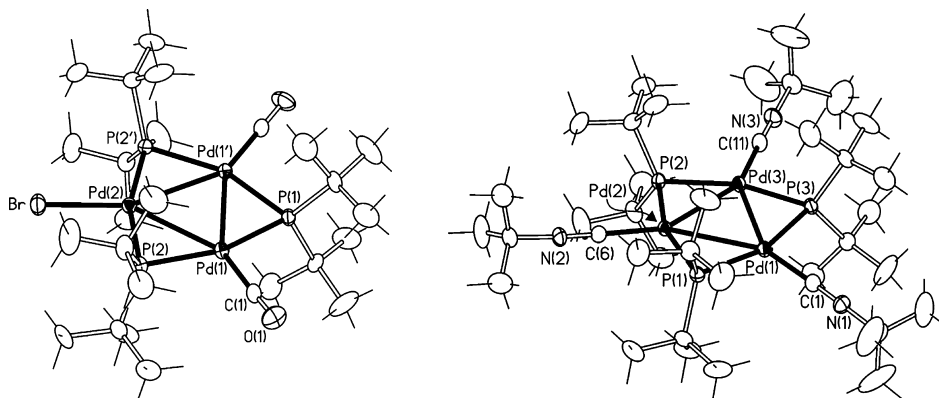
	Cluster	X	Y	n	ν^a	$\delta_{\text{P}_1\text{P}_2/\text{Hz}}$	$\delta_{\text{P}_2\text{P}_1/\text{Hz}}$
	2	Br	CO	0	2040	206.4 t (116)	282.7 d (116)
	3	I	CO	0	2034 (2049)	213.4 t (116)	292.5 d (116)
	4	Cl	CO	0	2038	204.8 t (115)	277.4 d (115)
	(5) PF_6	CO	CO	1	2094, 2053 (2079)	295.6 s	
	(6)I	CN ^{<i>n</i>} Bu	CN ^{<i>n</i>} Bu	1	2156 (2164)	257.2 s	
	(6)(PF_6) ₂	CN ^{<i>n</i>} Bu	CN ^{<i>n</i>} Bu	2	2193 (2188)	-	
	(7) PF_6	CH_3CN	CO	1	2058, 2044 (2067)	245.4 t (128)	275.8 d (128)
	(8) PF_6	Py	CO	1	2066	250.8 t (121)	258.9 d (121)

^a $\nu(\text{CO})$ in 2–4, (5) PF_6 , (7) PF_6 and (8) PF_6 ; $\nu(\text{CN})$ in (6)I and (6) PF_6 .

Table 2. Selected Bond Distances (Å) and Angles (deg) in the Structures of Clusters 2 and (6) CF_3SO_3

	2: <i>Pnma</i>	4: ^a <i>Pnma</i>	(6)CF ₃ SO ₃ : <i>P</i> ₂ /n	
Pd(1)–Pd(1)′	2.9960(13)	3.000(5)	Pd(1)–Pd(2)	2.9526(6)
Pd(1)–Pd(2)	2.9474(10)	2.949(6)	Pd(1)–Pd(3)	3.0056(6)
P(1)–Pd(1)	2.314(2)	2.315(2)	Pd(2)–Pd(3)	2.9683(6)
P(2)–Pd(1)	2.298(2)	2.305(2)	Pd(1)–P(1)	2.2941(16)
P(2)–Pd(2)	2.273(2)	2.273(10)	Pd(1)–P(3)	2.2950(16)
Pd(1)–C	1.874(10)	1.888(10)	Pd(1)–C(1)	1.947(7)
C–O	1.124(11)	1.109(10)	Pd(2)–C(6)	1.933(6)
Pd(2)–X	2.4601(16)	2.343(10)	Pd(3)–C(11)	1.950(7)
Pd(1)–Pd(2)–Pd(1)′	61.10(3)	61.15(4)	Pd(2)–Pd(1)–Pd(3)	59.752(15)
Pd(2)–Pd(1)–Pd(1)′	59.452(15)	59.43(4)	P(1)–Pd(2)–Pd(1)	49.93(4)
Pd(1)–P(1)–Pd(1)′	80.69(10)	80.78(6)	Pd(1)–P(1)–Pd(2)	80.01(5)
Pd(1)–P(2)–Pd(2)	80.30(7)	80.20(7)	N(3)–C(11)–Pd(3)	177.5(6)
P(2)–Pd(2)–X	99.24(6)	99.1(3)	C(6)–Pd(2)–P(1)	100.35(18)
P(2)–Pd(2)–Pd(1)	50.22(6)	50.38(7)	C(6)–N(2)–C(7)	176.1(8)
Pd(1)–C–O	177.5(9)	178.4(9)		

^aData for the structure of 4 are taken from ref 5.

Figure 1. ORTEP views of the molecular structure of cluster 2 (left) and of cation 6⁺ (right). Thermal ellipsoids are at 20% probability.

show signals, whereas the ^1H NMR spectrum contains only a very broad signal, due to the *tert*-butyl protons, at ca. 16 ppm.

The $^{31}\text{P}\{^1\text{H}\}$ NMR spectra of the neutral complexes 2–4 and of the cationic derivatives (7) PF_6 and (8) PF_6 contain low-field signals assigned to the equivalent nuclei P_2 and to P_1 . The symmetrical cationic clusters (5) PF_6 and (6) X [$\text{X} = \text{I}, \text{PF}_6, \text{CF}_3\text{SO}_3$] show only a singlet due to the three equivalent P nuclei. Ionic compounds containing the PF_6^- anion show also the expected heptet at ca. -140 ppm ($J_{\text{PF}} = \text{ca. } 700$ Hz).^{12,13} The ^1H NMR and $^{13}\text{C}\{^1\text{H}\}$ NMR spectra show signals with the expected frequencies and intensities (see the Experimental Section for more details).

2.2. Crystal and Molecular Structures. Single crystals of 2 suitable for crystallographic studies were obtained by slow evaporation from hexane solutions. Single crystals of (6)- CF_3SO_3 were obtained by layering *n*-hexane on a CH_2Cl_2 solution of the cluster.

Selected bond distances and angles are reported in Table 2, and ORTEP projections of the molecular structures are shown in Figure 1. Cluster 2 belongs to the $Pnma$ space group, and its structure is similar to the one reported⁵ for the isotopic chloro derivative 4. The coordination neighborhood of the palladium centers is planar, the maximum deviation [$\text{P}(1)$] being 0.19 Å. The asymmetric unit contains half a molecule with a mirror

Table 3. Formal Electrode Potentials (V vs SCE) and Peak-to-Peak Separations (mV) for the Redox Processes Exhibited in CH₂Cl₂ Solution by $[\{\text{Pd}_3\}\text{L}_{3-n}\text{X}_n]^{(1-n)+}$ and, for Comparison (in Parentheses), by the Corresponding Platinum Clusters $[\{\text{Pt}_3\}\text{L}_{3-n}\text{X}_n]^{(1-n)+}$

complex	oxidation processes				reduction processes	
	E°_1	ΔE_p^a	E°_2	ΔE_p^a	E°_3	
4	0.83 ^b (0.91) ^d	90 (70) ^d	0.41 (0.31) ^d	76 (60) ^d	−1.84 ^{a,c} , (−1.91) ^{c,d}	
2	0.90 ^{a,c} (0.88) ^d	(70) ^d	0.41 (0.29) ^d	80 (60) ^d	(−1.91) ^{c,d}	
3	0.85 (0.86) ^d	74 (70) ^d	0.38 (0.28) ^d	70 (70) ^d	−1.73 ^{a,c} (−1.91) ^{c,d}	
(5)PF ₆	1.75 ^{a,c} (1.56) ^d		1.14 (1.13) ^d	64 (90) ^d	−1.27 ^{a,c} (−1.29) ^{c,d}	
(6)PF ₆	1.14 (0.82) ^e	65 (65) ^e	0.35 (0.26) ^e	65 (65) ^e		
(7)PF ₆	1.50 ^{a,c}		0.79	70	−1.35 ^{a,c}	
(8)PF ₆	1.54 ^{a,c}		0.80	80	−1.36 ^{a,c}	

^aMeasured at 0.1 V s^{−1}. ^bCoupled to relatively fast chemical reactions. ^cPeak potential value for irreversible processes. ^dReference 2b. ^eUnpublished results for $[\text{Pt}_3(\mu\text{-PBUt}_2)_3(\text{CNBu}^t)_3]\text{PF}_6$.

plane passing through Br, Pd(2), P(1) and the two carbon atoms connected to P(1). The Pd₃ triangle is isosceles with two Pd(1)–Pd(2) distances [2.9474(10) Å] slightly shorter than the one opposing the bromide ligand [Pd(1)–Pd(1') 2.9960(13) Å]. The P(1) atom, bridging the longer Pd–Pd bond, shows Pd–P distances [Pd(1)–P(1) = 2.314(2) Å] slightly longer than the other ones [Pd(1)–P(2) = 2.298(2) Å and Pd(2)–P(2) = 2.273(2) Å]. The Pd(2)–Br distance [2.4601(16) Å] is almost coincident with the average calculated [2.456 Å] for ca. 180 known terminal bromides of palladium.¹⁴

Cation **6**⁺ belongs entirely to the asymmetric unit and does not show any rigorously valid symmetry operation. However, it locally approaches the 3*m* symmetry, C_{3v} in the Schönflies notation, which is not completely satisfied due to slight rotations of the *tert*-butyl groups of the isocyanide ligands. The molecule exhibits a scalene Pd₃ triangular core with two shorter and slightly different Pd(1)–Pd(2) and Pd(2)–Pd(3) bonds [2.9525(6) and 2.9686(6) Å, respectively] and one slightly longer Pd(1)–Pd(3) distance [3.0055(6) Å]. The Pd–P distances, between 2.293 and 2.299 Å, are similar to those found in **2**. The three isocyanide ligands are coordinated in an approximately linear fashion (Pd–C–N angles ca. 177°, C–N–C angles ca. 176°).

The Pd–C(isocyanide) distances [Pd(1)–C(1) = 1.947(6) Å, Pd(2)–C(6) = 1.936(6) Å, and Pd(3)–C(11) = 1.948(7) Å] are longer than the Pd–CO ones found in **2** [1.874(10) Å] but are similar to the corresponding distances in other trinuclear palladium clusters with terminal isocyanide ligands (i.e., Pd–C ca. 2.0 Å in $[\text{Pd}_3(\mu\text{-SO}_2)_2(\text{CNBu}^t)_2(\text{PBz}_3)_3]^{10}$ and Pd–C 1.94–2.06 Å in $[\text{Pd}_3(\mu\text{-PBUt}_2)_2(\text{CN}-\text{C}_6\text{H}_4\text{-}p\text{-Me})_5]^{11}$ and $[\text{Pd}_3(\mu\text{-PBUt}_2)_2(\text{CN}-\text{C}_6\text{H}_4\text{-}p\text{-Me})_5]^{11}$). As compared to the known⁵ structures of cluster **4** and of the numerous parent platinum derivatives $[\text{Pt}_3(\mu\text{-PBUt}_2)_3\text{L}_{3-n}\text{X}_n]^{(1-n)+}$ (*n* = 0, 1),^{1–4} the main features of the Pd₃(μ-PBUt₂)₃ core remain roughly unchanged, with the Pd, P, CN (in cation **6**⁺) virtually on the same plane (maximum deviation 0.19 Å in **6**⁺ [P(2)]). The central Pd₃ triangle is nearly equilateral with quite long Pd–Pd distances (ca. 3 Å) well-matched with the M–M bond order (0.66) expected¹⁵ for mixed valence derivatives of this type. Pd–P, Pd–C, and Pd–halogen bond distances fall in the range observed for the corresponding moieties in the literature.

2.3. Electrochemistry. The electrochemical properties of the clusters were studied by cyclic voltammetry in CH₂Cl₂ solutions containing [ⁿBu₄N]PF₆ (0.2 mol dm^{−3}) as the supporting electrolyte.

Two sequential monoelectronic oxidations, typifying the redox fingerprint of the analogous 44e[−] $[\{\text{Pt}_3\}\text{L}_{3-n}\text{X}_n]^{(1-n)+}$

clusters,^{2b} were observed also in the cyclic voltammograms of the palladium clusters described here. The former is reversible in the CV time scale, while the second oxidation is reversible only for clusters **3** and **6**⁺ and complicated by a subsequent chemical reaction for all the others. In the cathodic region, one irreversible reduction is observed for several compounds. The formal electrode potentials for the observed electron transfers are summarized in Table 3, and the CV profiles of **3**, **5**⁺, and **6**⁺ are shown in Figure 2.

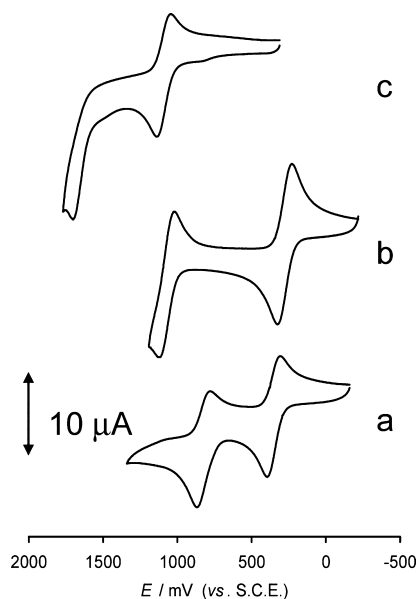


Figure 2. Cyclic voltammograms recorded at a platinum electrode in CH₂Cl₂ solutions of (a) **3**, (b) **6**⁺, and (c) **5**⁺. [ⁿBu₄N]PF₆ (0.2 mol dm^{−3}) as supporting electrolyte. Scan rates: 0.2 V s^{−1}.

The neutral monohalide clusters **2**–**4** are oxidized in two steps at ca. 0.40 and 0.85 V, the first oxidation being fully reversible on the CV time scale (*i_c/i_a* = 1 at 0.2 V s^{−1}); the second one is reversible for **3** while, for **2** and **4**, it is complicated by a subsequent chemical reaction.

As expected for the presence of the positive charge and for the substitution of a σ-donor halide with a π-acid carbonyl ligand, the two oxidations occur at higher potentials (+1.14 and +1.75 V) for the cationic tricarbonyl derivative (**5**)PF₆. The substitution of one of the carbonyl ligands in **5**⁺ with a good σ-donor as an acetonitrile or a pyridine molecule facilitates the removal of both the first (0.79 for **7**⁺ and 0.80 V for **8**⁺) and the

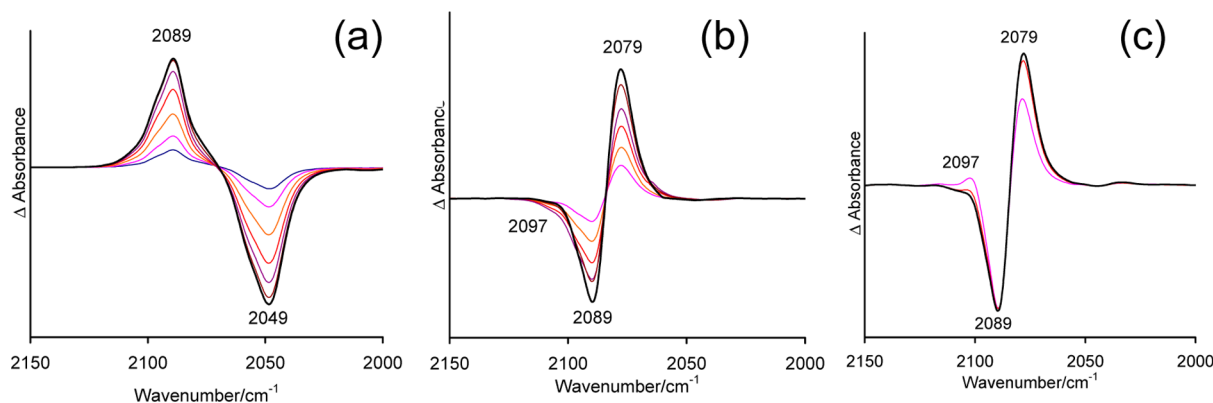
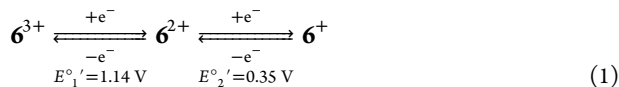


Figure 3. IR spectral changes recorded in an OTTLE cell (a) during and (b) immediately and (c) 30 min after the progressive one electron oxidation of **3** in CH_2Cl_2 with $[\text{Bu}_4\text{N}]\text{PF}_6$ (0.2 mol dm^{-3}) as the supporting electrolyte. A reference spectrum, collected before the application of an oxidation potential, is used to calculate the differential absorbance spectra (a). The final spectrum, giving the differential spectrum represented by the black line in panel a, is used to calculate the differential absorbance spectra (b and c).

second electron (1.50 for 7^+ and 1.54 V for 8^+). Again, for either 5^+ , 7^+ , or 8^+ , the first oxidation is reversible on the CV time scale ($i_c/i_a = 1$ at 0.2 V s^{-1}) and the second oxidation is followed by a fast chemical reaction. Moreover, cations 7^+ and 8^+ slowly decompose in CH_2Cl_2 solution, and, on standing, redox processes attributable to decomposition products become evident in the CV profile. Finally the cationic cluster $(6)\text{PF}_6$, with three good σ -donor and relatively poor π -acid alkyl-isocyanide ligands, and its oxidation products distinguish themselves for their remarkable stability.

In spite of the positive charge and compared to all the clusters analyzed in this study, the removal of the first electron occurs at the lowest potential (+0.35 V). The potential of the second oxidation (+1.14 V) is lower than those of the other cations but is higher in comparison to those of the neutral derivatives **2–4**. Both oxidation processes possess features of chemical reversibility in the CV time scale. $(6)\text{I}$ behaves as $(6)\text{PF}_6$, showing two reversible oxidations in the CV time scale, although the first process is superimposed to the oxidation of I^- .

It is worth noting that only for cluster **3** and cation 6^+ both oxidation processes are reversible in the CV time scale and, furthermore, 6^+ exhibits the largest ΔE° gap ($E^\circ_1 - E^\circ_2 = 0.79 \text{ V}$). This value points to a large thermodynamic stability for the mono-oxidized species 6^{2+} , as indicated by the large comproportionation constant K_c (ca. 10^{13} , eqs 1, 2)¹⁶ and experimentally confirmed by the above-mentioned isolation of the thermally stable $43e^-$ species $(6)(\text{PF}_6)_2$.



$$K_c = \frac{[6^{2+}]^2}{[6^{3+}][6^+]} = e^{F\Delta E^\circ/RT} = 2.26 \times 10^{13} \quad (2)$$

Most of the half-wave potentials shown in Table 3 are shifted anodically in comparison with the corresponding potentials of their platinum analogues; thus the latter are easier to oxidize and harder to reduce. The shift is generally significant ($E^\circ_n(\text{Pd}) - E^\circ_n(\text{Pt}) = 70\text{--}190 \text{ mV}$) and in one case quite large (320 mV for E°_1 of cation 6^+), although, occasionally, also very small (10–20 mV) or even reversed shifts (–10 and –80 mV for E°_1 of clusters **3** and **4**, respectively) were observed. A similar trend in the redox potentials of homologous series of Pt and Pd

complexes has been observed previously^{17,18} and has been assigned to the higher softness^{17a} of platinum. In some cases a broad agreement has been found between the experimental peak potential differences and variations of the calculated energies of the HOMO and LUMO orbitals, both of which were found to increase when exchanging Pd with Pt.^{17b}

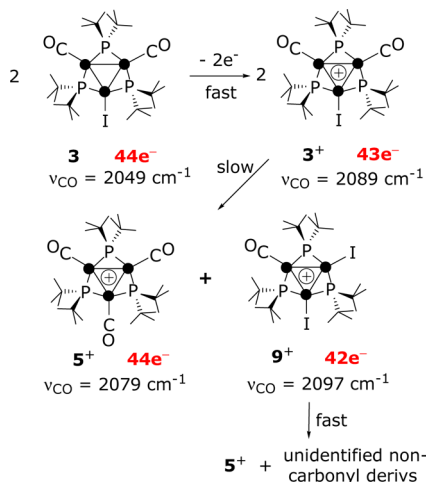
Contrary to our clusters, and despite the lower average Pd oxidation state (Pd_3^{2+} instead of Pd_3^{4+}), the tris-dppm bridged trinuclear dication $[\text{Pd}_3(\mu_2\text{-dppm})_3(\text{CO})]^{2+}$ (dppm = bis-(diphenylphosphino)methane) gives stable species upon reduction and decomposes upon oxidation. In fact, its CV profile exhibits monoelectronic reduction processes at –0.21, –0.47, and –2.35 V (reversible) and at –2.69 V (irreversible) in THF¹⁹ and two irreversible 2-electron oxidations at +0.95 and +1.15 V in CH_3CN .¹⁹ The instability of the oxidized species in these cases is reasonably due to an unbearable concentration of positive charge.

2.4. Spectroelectrochemistry. 2.4.1. Cluster 3. Even though the first monoelectronic oxidation of **3** is reversible in the CV time scale, the lability of the electrogenerated species 3^+ becomes evident in the longer times of the macroelectrolysis experiments ($E_w = +0.5 \text{ V}$). In fact, during the exhaustive electrolysis, the CV of the solution shows that the accumulation of the oxidized species 3^+ is accompanied by a decrease of the total concentration of the $3/3^+$ couple, while new peaks become evident: a reversible oxidation at 1.14 V, two reversible reductions at –0.27 and –0.52 V, and three irreversible reductions at –0.87, –1.16, and –1.27 V. The UV–vis and IR spectroelectrochemical changes following the oxidation of **3** in correspondence of the first oxidation process show the presence of well-defined isosbestic points for the time required for the quasi-complete oxidation of **3**, suggesting the initial formation of a metastable cation 3^+ that is then consumed by a subsequent reaction. As illustrated in Figure 3a, the CO stretching absorption exhibited by **3** at 2049 cm^{-1} vanishes rapidly upon oxidation while a new absorption, assigned to the $43e^-$ species 3^+ , grows at 2089 cm^{-1} .

This band is then slowly replaced (Figure 3b) by a new absorption at 2079 cm^{-1} , that can be unambiguously assigned to the $44e^-$ tricarbonyl cation 5^+ (by comparison of its IR, UV, and ^{31}P NMR signals with those of an authentic sample and by the above-mentioned CV peaks at +1.14 and –1.27 V observed after electrolysis), and by a transient absorption at 2097 cm^{-1} (Figure 3b,c), that we tentatively assign to the $42e^-$ cluster

$[\text{Pd}_3(\mu\text{-PBUt}_2)_3(\text{CO})\text{I}_2]^+$, 9^+ . As highlighted in Scheme 3, 2 equiv of the metastable oxidized species 3^+ could produce a 1:1

Scheme 3. Possible Pathway to the Mixture of Cations 5^+ and 9^+



mixture of 5^+ and 9^+ , but the latter does not accumulate due to its rapid decomposition. According to this picture, the small upfield shift of 8–10 cm^{-1} per removed electron, observed for the value of ν_{CO} in the series 5^+ ($44e^-$) \rightarrow 3^+ ($43e^-$) \rightarrow 9^+ ($42e^-$), may be assigned to the substitution of a π -acceptor carbonyl with a σ -donor iodide in each step (which, furthermore, leaves unchanged the total charge in spite of the oxidation). This process nearly counterbalances the reduction of π -basicity of the metal centers caused by the removal of electrons. Unfortunately, the full characterization of 9^+ was prevented by its fast decomposition (Figure 3c), which proceeds by forming, among other products, a further amount of 5^+ . The latter is the only carbonyl species that was detected in solution after exhaustive electrolysis, when the IR spectrum shows a unique carbonyl absorption at 2079 cm^{-1} . The $^3\text{P}\{^1\text{H}\}$ NMR spectrum of this solution contains an intense singlet at 295.6 ppm, due to 5^+ (Table 1), together with several weak singlets for unidentified noncarbonyl derivatives in the region between 0 and 200 ppm. The UV–vis spectroelectrochemistry (Figure 4) agrees with this picture: the broad absorption at 464 nm observed in the original sample of 3 decreases during electrolysis at +0.5 V, while three new bands at 555, 592, and

643 nm, assigned to 3^+ , keep growing. Their intensity increases until cluster 3 has nearly disappeared at the end of the current flow in the cell. The absorbance changes observed after this step confirm the decay of 3^+ : the three absorptions at 555, 592, and 643 nm are replaced by two bands at 441 and 635 nm, the former of which is consistent with the formation of cluster 5^+ while the second may be assigned to unidentified decomposition compounds. The pathway outlined in Scheme 3 is also suggested by some analogies and differences that have been found in the behavior of complex 3 and of its platinum analogue, $\text{Pt}_3(\mu\text{-PBUt}_2)_3(\text{CO})_2\text{I}$, 10 ,²⁰ which may be reversibly oxidized (chemically or electrochemically) to its corresponding $43e^-$ monocation 10^+ .

Although, contrary to 3^+ , this species is *thermally stable*, in the presence of an excess of I^- it undergoes CO/ I^- scrambling and electron transfer to afford, initially, a 1:1 mixture of $[\text{Pt}_3(\mu\text{-PBUt}_2)_3(\text{CO})_3]^+$, the Pt equivalent of the $44e^-$ derivative 5^+ , and of the first tris-phosphido-bridged triangular cluster of platinum stable with 42 instead of $44e^-$, namely, $\text{Pt}_3(\mu\text{-PBUt}_2)_3\text{I}_3$, which has been isolated as a stable crystalline solid and fully characterized. In the presence of I^- , which reacts with $[\text{Pt}_3(\mu\text{-PBUt}_2)_3(\text{CO})_3]^+$ to regenerate cluster 10 , and of the oxidant, the reaction continues until complete conversion of $\text{Pt}_3(\mu\text{-PBUt}_2)_3(\text{CO})_2\text{I}$ into $\text{Pt}_3(\mu\text{-PBUt}_2)_3\text{I}_3$.²⁰

The results described here suggest that any $42e^-$ Pd_3 species, including the hypothetical cluster $\text{Pd}_3(\mu\text{-PBUt}_2)_3\text{I}_3$ which could simply be formed by the reaction of 9^+ with I^- , would not be easily isolable.

As expected, by performing the IR spectroelectrochemical analysis of 3 in the presence of an excess of $[\text{nBu}_4\text{N}]\text{I}$, which converts back rapidly 5^+ into cluster 3 , we observed the appearance of *only* the transient absorption assigned to cation 9^+ and, eventually, complete decomposition to a complex mixture of noncarbonyl derivatives. Moreover, after an exhaustive electrolysis, the CV of the solution shows two weak waves for reversible reductions in the cathodic region (−0.27 and −0.88 V),²¹ that we may tentatively assign to the unstable cation 9^+ . We recall that the redox potentials for the related reductions of $[\text{Pt}_3(\mu\text{-PBUt}_2)_3(\text{CO})\text{I}_2]^+$, 11^+ , the elusive platinum analogue of cation 9^+ , were estimated to be +0.06 ($11^{+/0}$) and −0.47 ($11^{0/-1}$) V.²⁰

2.4.2. Cation 5^+ . IR and UV–vis in situ spectroelectrochemical experiments on CH_2Cl_2 solutions of 5^+ allowed the characterization of the product of its monoelectronic oxidation 5^{2+} . Upon oxidation, the ν_{CO} absorption of 5^+ at 2079 cm^{-1} is

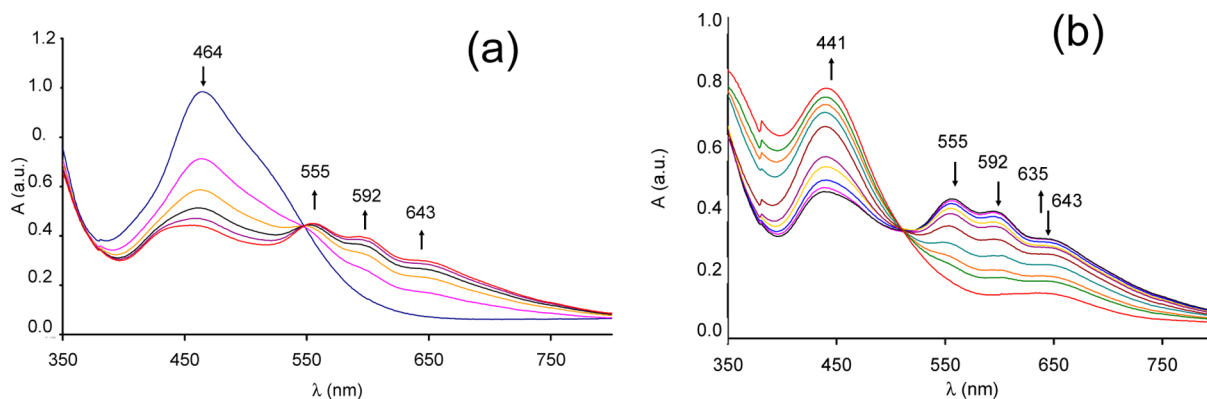


Figure 4. UV–vis spectra of 3 in CH_2Cl_2 solution containing $[\text{nBu}_4\text{N}]\text{PF}_6$ (0.2 mol dm^{-3}) as the supporting electrolyte recorded in an OTTLE cell (a) during and (b) after one electron oxidation.

gradually replaced by a new band at 2115 cm^{-1} (Figure 5). On the time scale of the IR experiment, however, the oxidation is

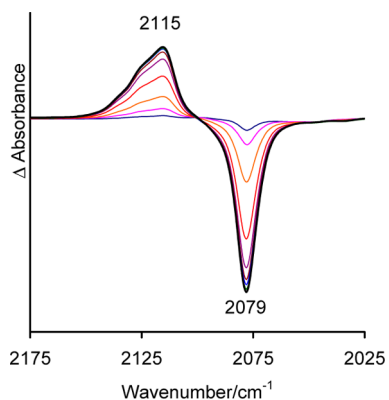


Figure 5. IR spectral changes recorded in an OTTLE cell during the progressive one electron oxidation of 5^+ in CH_2Cl_2 solution; $[\text{Bu}_4\text{N}]\text{PF}_6$ (0.2 mol dm^{-3}) as the supporting electrolyte. A reference spectrum, collected before the application of an oxidation potential, is used to calculate the differential absorbance spectra.

followed by a partial decomposition that did not allow the complete recovery of the starting compound in the backward reduction of 5^{2+} . The removal of one electron from 5^+ produces a markedly different pattern of the absorption bands in the visible region of the electronic spectrum (Figure 6). The 441 nm band of the starting cluster is substituted, during the course of the spectroelectrochemical oxidation, by three new absorptions at 521 , 555 , and 710 nm .

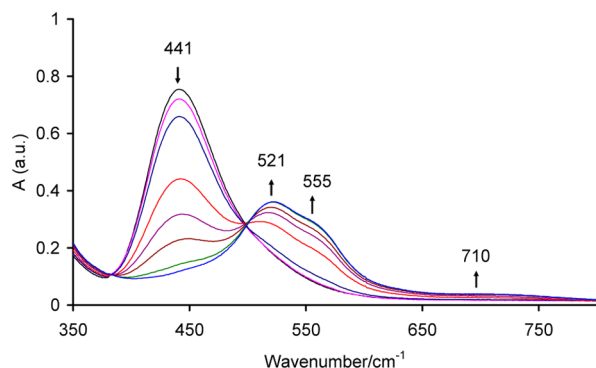


Figure 6. UV-vis spectra of 5^+ in CH_2Cl_2 solution containing $[\text{Bu}_4\text{N}]\text{PF}_6$ (0.2 mol dm^{-3}) as the supporting electrolyte recorded in an OTTLE cell during one electron oxidation.

2.4.3. Cation 6^+ . The IR spectroelectrochemical changes following the stepwise two-electron oxidation of cation (6) PF_6 (Figure 7) show the appearance of well-defined and withstanding isosbestic points and confirm a remarkable stability of the oxidized clusters 6^{2+} and 6^{3+} . The ν_{CN} absorptions exhibit a linear upfield shift of 24 cm^{-1} per removed electron: the original absorption found at 2164 cm^{-1} in 6^+ moves to 2188 cm^{-1} upon one electron oxidation, and to 2212 cm^{-1} after removal of the second electron.

Quantitative restoration of the IR band of the starting 6^+ was observed in the backward reduction step. The stepwise oxidation of 6^+ in a UV-vis spectroelectrochemical experiment is shown in Figure 8. Only the removal of the first electron gives rise to evident spectral changes: the disappearance of the

421 nm band due to 6^+ is accompanied by the growth of an absorption at 524 nm together with a weak band at 690 nm .

3. CONCLUSIONS

After this work a new class of palladium triangular clusters with three bridging phosphides, that was practically unknown before, becomes available to the inorganic chemistry community. Although, as expected, these clusters are somewhat less stable than their well-known platinum analogues, they can be prepared in high yield and purity and can be stored for further studies. The presence of easily displaceable terminal ligands as acetonitrile, pyridine, or even the halides, is expected to allow many different types of functionalization of the relatively stable $\{\text{Pd}_3\}$ core. Moreover, cationic $[\{\text{Pd}_3\}(\text{L})_3]^+$ systems have three identical ligands lying at 120° on the molecular plane, and in neutral $\{\text{Pd}_3\}(\text{L})_2\text{X}$ derivatives the reactivity of the L and X ligands is substantially different. All these features make these systems well-suited to be employed as branching points or as end-caps in polycluster macromolecular structures in which the cluster-to-cluster connection can be effected, for example, with 4,4'-dipyridyl or bis-isocyanide ligands. The reversibility of the first monoelectronic oxidation process and the remarkable stability of the resulting paramagnetic $43e^-$ species, particularly high in the isocyanide clusters, may allow the construction of ordered and stable polyradical frameworks, in which the spin-spin intercluster interactions may be triggered by modifying the nature of the spacer.

4. EXPERIMENTAL SECTION

4.1. General Data. The reactions were carried out under a nitrogen atmosphere, using standard Schlenk techniques. $[\text{Pd}(\text{PBu}_2\text{H})(\mu\text{-PBu}_2)_2]_2$ (**1**)⁹ and decamethylferrocene²² were prepared according to the literature. $[\text{Bu}_4\text{N}]\text{Br}$, $[\text{Bu}_4\text{N}]\text{I}$, AgBF_4 , $\text{Ag}[\text{CF}_3\text{SO}_3]$, $[(\text{PPh}_3)_2\text{N}]\text{Cl}$, CNBu' , purchased from Sigma Aldrich, and TIPF_6 , purchased from Apollo Scientific, were used as received. Solvents were dried by refluxing over the appropriate drying agent [sodium/benzophenone (toluene, thf, Et_2O , *n*-pentane, *n*-hexane); CaH_2 (CH_3CN , pyridine); K_2CO_3 (acetone)] and distilled under nitrogen prior to use. Deuterated solvents were purchased from Cambridge Isotope Laboratories and were used without further purification but were deoxygenated by freeze-pump-thaw cycles and stored over 4 \AA molecular sieves under an inert atmosphere. IR spectra were recorded on a Perkin-Elmer FT-IR 1725X or a Spectrum 100 FT-IT spectrophotometer. NMR spectra were recorded on a Varian Gemini 200 BB instrument; frequencies are referenced to the residual resonances of the deuterated solvent (^1H , ^{13}C) or 85% H_3PO_4 (^{31}P). UV-vis spectra were recorded on a Perkin-Elmer Lambda EZ201 spectrophotometer. Molecular hydrogen evolved during the reactions was detected by gas chromatographic analysis performed with a DANI 3200 instrument equipped with a D-SM 5A column.

4.2. Electrochemistry and Spectroelectrochemistry. Electrochemical measurements were recorded on a Princeton Applied Research (PAR) 273A potentiostat/galvanostat and were performed in dichloromethane solutions containing $[\text{Bu}_4\text{N}]\text{PF}_6$ (0.2 mol dm^{-3}) as the supporting electrolyte. HPLC grade dichloromethane (Sigma-Aldrich) was stored under argon over 3 \AA molecular sieves. Electrochemical grade $[\text{Bu}_4\text{N}]\text{PF}_6$ was purchased from Fluka and used without further purification. Cyclic voltammetry was performed in a three-electrode cell, having a platinum reference electrode, a platinum-spiral counter electrode, and a platinum-disk working electrode, and containing a $5 \times 10^{-4}\text{ M}$ analyte solution. After a sufficient number of voltammograms were recorded, a small amount of decamethylferrocene was added to the solution and a further voltammogram was recorded. Potential values were determined by placing the redox couple decamethylferrocenium/decamethylferrocene [E_{redox} calculated as $(E_{\text{pc}} + E_{\text{pa}})/2$] at -0.16 V vs SCE. Controlled

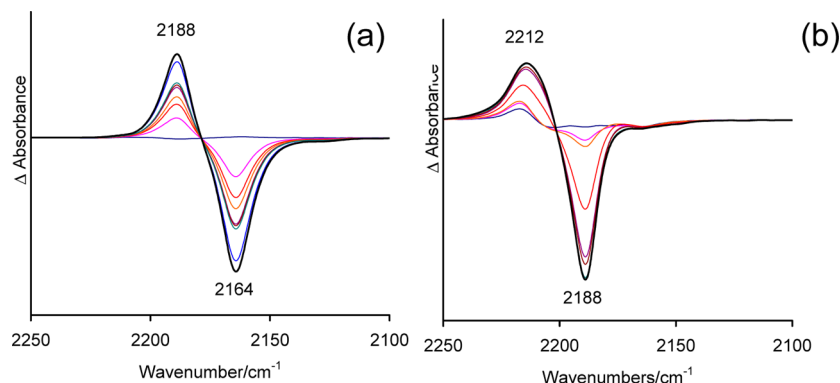


Figure 7. IR spectral changes recorded in an OTTLE cell during the first (a) and the second (b) mono-electronic oxidation of 6^+ in CH_2Cl_2 solution, with $[\text{nBu}_4\text{N}]\text{PF}_6$ (0.2 mol dm^{-3}) as the supporting electrolyte. A reference spectrum, collected before the application of an oxidation potential, was used to calculate the differential absorbance spectra (a). The final spectrum, giving the differential spectrum represented by the black line in panel a, is used to calculate the differential absorbance spectra (b).

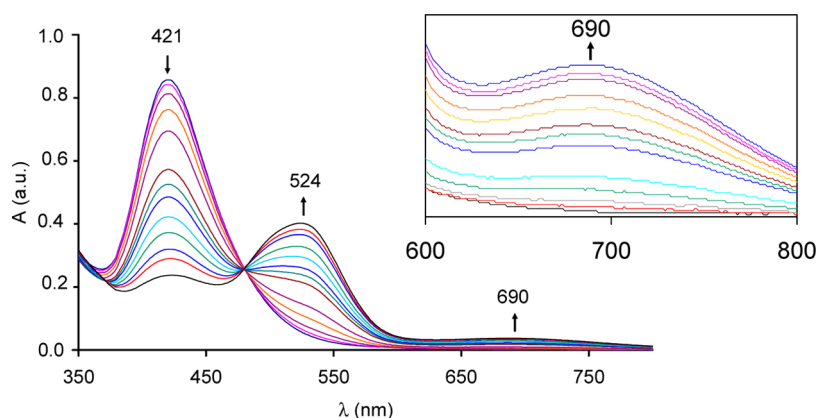


Figure 8. UV-vis spectra of 6^+ in CH_2Cl_2 solution containing $[\text{nBu}_4\text{N}]\text{PF}_6$ (0.2 mol dm^{-3}) as the supporting electrolyte recorded in an OTTLE cell during one electron oxidation.

potential coulometry was performed in an H-shaped cell with anodic and cathodic compartments separated by a sintered-glass disk. The working macroelectrode was a platinum gauze; a platinum-spiral was used as the counter electrode.

UV-vis and infrared (IR) spectroelectrochemical measurements were carried out using an optically transparent thin-layer electrochemical (OTTLE) cell equipped with CaF_2 windows, platinum minigrid working and auxiliary electrodes, and silver wire pseudoreference electrode.²³ Controlled-potential electrolyses were carried out with a BAS CV-27 electrochemical analyzer. Argon-saturated CH_2Cl_2 solutions (10^{-3} M or 10^{-2} M for UV-vis or IR analysis, respectively) of the compound under study, containing $[\text{nBu}_4\text{N}]\text{PF}_6$ 0.2 M as the supporting electrolyte, were used. The in situ spectroelectrochemical experiments have been performed by collecting spectra of the compound under investigation during the stepwise oxidation obtained by increasing the initial working potential by ΔE steps of 25 mV ($\Delta t = 1$ or 2 min for IR or UV-vis analysis, respectively).

4.3. Synthesis of $\text{Pd}_3(\mu\text{-PBu}^t)_3(\text{CO})_2\text{Br}$ (2). $[\text{nBu}_4\text{N}]\text{Br}$ (39 mg, 0.12 mmol) and H_2O (0.5 mL) were added to a suspension of complex **1** (145 mg, 0.18 mmol) in toluene (10 mL). The flask was then filled with CO (1 atm), and the reaction mixture was stirred for 3 days at 100°C . The solid residue was filtered off, and the remaining red solution was evaporated. The residue was purified by column chromatography on neutral alumina (hexane–acetone 20:1) yielding 67 mg (0.076 mmol , 63% yield) of **2** as red solid. $^1\text{H NMR}$ (200 MHz , C_6D_6 , 293 K): δ (ppm) = 1.47 (vt, $^3J(\text{H,P}) + ^5J(\text{H,P}) = 7.1 \text{ Hz}$, CCH_3 , 36 H), 1.13 (d, $^3J(\text{H,P}) = 14.6 \text{ Hz}$, CCH_3 , 18 H). $^{13}\text{C}\{^1\text{H}\}$ NMR (50.3 MHz , C_6D_6 , 293 K): δ = 188.6 (s, CO), 40.8 , 38.9 (s, PC-CH_3), 33.3 , 29.9 ppm (s, PC-CH_3). $^{31}\text{P}\{^1\text{H}\}$ NMR (81.0 MHz , C_6D_6 , 293 K): δ = 282.7 (d, $^2J(\text{P,P}) = 116 \text{ Hz}$, 2 P), 206.4 ppm (t, $^2J(\text{P,P}) = 116 \text{ Hz}$, 1

P). IR (solid state): 2040 ($\nu_{\text{C}\equiv\text{O}}$) cm^{-1} . Elemental analysis calcd (%) for $\text{C}_{26}\text{H}_{54}\text{O}_2\text{P}_3\text{Pd}_3\text{Br}$: C 35.1, H 6.11. Found: C 34.9, H 6.13.

In a separate experiment, a solution of KBr (18 mg ; 0.151 mmol) in H_2O (1 mL) was added to a suspension of complex **1** (124 mg , 0.156 mmol) in toluene (10 mL) under 1 atm of CO . After stirring for 3 days at 100°C the color of the solution turned red, while H_2 was evolved (GC). At the end of the reaction the aqueous phase turned basic and the $^{31}\text{P}\{^1\text{H}\}$ NMR spectrum of the toluene solution showed the presence of free PBu_2H and **2** in ca. 3:1 ratio as the predominant products. After workup according to the precedent procedure, **2** was isolated as a red solid (56 mg ; 0.063 mmol , 60% yield).

4.4. Synthesis of $\text{Pd}_3(\mu\text{-PBu}^t)_3(\text{CO})_2\text{I}$ (3). $[\text{nBu}_4\text{N}]\text{I}$ (51 mg , 0.139 mmol) and H_2O (0.5 mL) were added to a suspension of complex **1** (166 mg , 0.208 mmol) in toluene (15 mL); the flask was filled with CO (1 atm), and the reaction mixture was stirred for 3 days at 100°C . The solid residue was filtered off, and the remaining red solution was evaporated. The residue was purified by column chromatography on neutral alumina (hexane–acetone 20:1). Yield: 85% (110 mg , 0.12 mmol) of red solid. $^1\text{H NMR}$ (200 MHz , C_6D_6 , 293 K): δ = 1.50 (vt, $^3J(\text{H,P}) + ^5J(\text{H,P}) = 7.0 \text{ Hz}$, CCH_3 , 36 H), 1.13 ppm (d, $^3J(\text{H,P}) = 14.5 \text{ Hz}$, CCH_3 , 18 H). $^{13}\text{C}\{^1\text{H}\}$ NMR (50.3 MHz , C_6D_6 , 293 K): δ = 188.4 (s, CO), 41.1 , 39.1 (s, PC-CH_3), 34.2 , 33.3 ppm (s, PC-CH_3). $^{31}\text{P}\{^1\text{H}\}$ NMR (81.0 MHz , C_6D_6 , 293 K): δ = 292.5 (d, $^2J(\text{P,P}) = 116 \text{ Hz}$, 2 P), 213.4 ppm (t, $^2J(\text{P,P}) = 116 \text{ Hz}$, 1 P). IR (CH_2Cl_2): 2049 ($\nu_{\text{C}\equiv\text{O}}$) cm^{-1} . IR (solid state): 2034 ($\nu_{\text{C}\equiv\text{O}}$) cm^{-1} . Elemental analysis calcd (%) for $\text{C}_{26}\text{H}_{54}\text{O}_2\text{P}_3\text{Pd}_3\text{I}$: C 33.3, H 5.80. Found: C 33.1, H 5.85.

In a separate experiment, a solution of KI (18 mg ; 0.151 mmol) in H_2O (1 mL) was added to a suspension of complex **1** (156 mg , 0.196 mmol) in toluene (10 mL) under 1 atm of CO . After stirring for 3

days at 100 °C the color of the solution turned red, while H₂ was evolved (GC). At the end of the reaction the aqueous phase turned basic and the ³¹P{¹H} NMR spectrum of the toluene solution showed the presence of free PBu₂H and **3** in ca. 3:1 ratio as the predominant products. After workup according to the precedent procedure, **3** was isolated as a red solid (102 mg, 0.109 mmol, 83% yield).

4.5. Synthesis of [Pd₃(μ-PBu₂)₃(CO)₃]PF₆, (5)PF₆. TlPF₆ (67 mg, 0.19 mmol) was added to a solution of **3** (90 mg, 0.096 mmol) in 25 mL of dry THF. The red solution was stirred overnight under 1 atm of carbon monoxide. TlI was filtered off, and the solvent was evaporated. The crude residue was washed with hexane and vacuum-dried. 73 mg of (5)PF₆ (0.074 mmol) was obtained as a reddish solid, yield 77%. ¹H NMR (200 MHz, acetone-*d*₆, 293 K): δ = 1.42 ppm (vt, ³J(H,P) + ⁵J(H,P) = 7.5 Hz, CCH₃, 54 H). ¹³C{¹H} NMR (50.3 MHz, acetone-*d*₆, 293 K): δ = 185.8 (s, CO), 42.4 (s, PC-CH₃), 33.5 ppm (s, PC-CH₃). ³¹P{¹H} NMR (81.0 MHz, acetone-*d*₆, 293 K): δ = 295.6 (s, 3 P), -142.2 ppm (hept, ¹J(P,F) = 708 Hz, PF₆, 1 P). IR (CH₂Cl₂): 2079 (ν_{C=O}) cm⁻¹. IR (solid state): 2094, 2053 (ν_{C=O}) cm⁻¹. Elemental analysis calcd (%) for C₂₇H₅₄F₆O₃P₄Pd₃: C 33.0, H 5.53. Found: C 32.2, H 5.49.

4.6. Synthesis of Pd₃(μ-PBu₂)₃(CO)₂Cl (4). [(PPh₃)₂N]Cl (40 mg, 0.070 mmol) was added to a red solution of (5)PF₆ (69 mg, 0.070 mmol) in 5 mL of dry acetone, and the mixture was stirred for 1 h at room temperature. After this period, the solvent was evaporated and the residue was dissolved in 5 mL of *n*-pentane. A colorless solid was filtered off, and **4** was collected as a red solid after solvent evaporation (46 mg, 0.054 mmol, yield 77%). ¹H NMR (200 MHz, C₆D₆, 293 K): δ = 1.46 (vt, ³J(H,P) + ⁵J(H,P) = 7.1 Hz, CCH₃, 36 H), 1.12 ppm (d, ³J(H,P) = 14.6 Hz, CCH₃, 18 H). ¹³C{¹H} NMR (50.3 MHz, C₆D₆, 293 K): δ = 188.4 (s, CO), 40.6, 38.9 (s, PC-CH₃), 33.3, 32.9 ppm (s, PC-CH₃). ³¹P{¹H} NMR (81.0 MHz, C₆D₆, 293 K): δ = 277.4 (d, ²J(P,P) = 115 Hz, 2 P), 204.8 ppm (t, ²J(P,P) = 115 Hz, 1 P). IR (solid state): 2038 (ν_{C=O}) cm⁻¹. Elemental analysis calcd (%) for C₂₆H₅₄O₂P₃Pd₃Cl: C 36.9, H 6.43. Found: C 37.2, H 6.39.

4.7. Synthesis of [Pd₃(μ-PBu₂)₃(CNBu^t)₃]I, (6)I. CNBu^t (32 μL, 0.288 mmol) and complex **3** (90 mg, 0.096 mmol) were dissolved in 10 mL of toluene. Immediately an orange solid precipitated out. The mixture was stirred for a further 1 h, and the orange solid was filtered, washed with toluene (3 × 5 mL), and vacuum-dried (94 mg, 0.083 mmol, yield 87%). ¹H NMR (200 MHz, acetone-*d*₆, 293 K): δ = 1.32 (vt, ³J(H,P) + ⁵J(H,P) = 7.0 Hz, PCCH₃, 54 H), 1.72 ppm (s, CNCCH₃, 27 H). ¹³C{¹H} NMR (50.3 MHz, acetone-*d*₆, 293 K): δ = 137.4 (s, CN), 59.9 (s, NC-CH₃), 40.0 (s, PC-CH₃), 34.0 (s, PC-CH₃), 30.5 ppm (s, NC-CH₃). ³¹P{¹H} NMR (81.0 MHz, acetone-*d*₆, 293 K): δ = 257.2 (s, 3 P). IR (CH₂Cl₂): 2164 (ν_{C≡N}) cm⁻¹. IR (solid state): 2156 (ν_{C≡N}) cm⁻¹. Elemental analysis calcd (%) for C₃₉H₈₁N₃P₃Pd₃I: C 41.4, N 3.71, H 7.22. Found: C 41.2, N 3.69, H 7.25.

4.8. Synthesis of [Pd₃(μ-PBu₂)₃(CNBu^t)₃]PF₆, (6)PF₆. TlPF₆ (31 mg, 0.088 mmol) was added to a solution of (6)I (50 mg, 0.044 mmol) in CH₂Cl₂/THF 1:1 (3 mL), and the reaction mixture was stirred for 24 h at 40 °C. After this period, the solvent was evaporated under vacuum. The crude residue was then dissolved in CH₂Cl₂, and TlI was filtered off. (6)PF₆ was obtained as an orange solid (48 mg, 0.042 mmol, yield 95%) after solvent evaporation.

4.9. Synthesis of [Pd₃(μ-PBu₂)₃(CNBu^t)₃]CF₃SO₃, (6)CF₃SO₃. A stoichiometric amount of AgCF₃SO₃ (14 mg, 0.053 mmol) was added to a CH₂Cl₂ (3 mL) solution of (6)I (60 mg, 0.053 mmol). Immediately AgI precipitated out. (6)CF₃SO₃ was obtained as orange solid (57 mg, 0.049 mmol, 92% yield), after removal of the salt by filtration and solvent evaporation.

4.10. Synthesis of [Pd₃(μ-PBu₂)₃(CO)₂(NCCH₃)]PF₆, (7)PF₆. TlPF₆ (52 mg, 0.149 mmol) was added to a solution of **3** (70 mg, 0.075 mmol) in dry acetonitrile (3 mL); the mixture was stirred overnight at room temperature. TlI was filtered off, and the solvent was evaporated. The crude residue was washed with hexane and diethyl ether and vacuum-dried. Complex (7)PF₆ was obtained as a dark red solid (64 mg, 0.064 mmol, yield 86%). ¹H NMR (200 MHz, acetone-*d*₆, 293 K): δ = 2.90 (s, NCCH₃, 3 H), 1.40 (vt, ³J(H,P) + ⁵J(H,P) = 7.4 Hz, CCH₃, 36 H), 1.38 ppm (d, ³J(H,P) = 15.1 Hz,

CCH₃, 18 H). ¹³C{¹H} NMR (50.3 MHz, acetone-*d*₆, 293 K): δ = 185.2 (s, CO), 124.3 (s, NCCH₃), 41.7, 40.6 (s, PC-CH₃), 32.8, 32.3 (s, PC-CH₃), 2.6 ppm (s, NCCH₃). ³¹P{¹H} NMR (81.0 MHz, acetone-*d*₆, 293 K): δ = 275.8 (d, ²J(P,P) = 128 Hz, 2 P), 245.4 (t, ²J(P,P) = 128 Hz, 1 P), -137.1 ppm (hept, ¹J(P,F) = 697 Hz, PF₆, 1 P). IR (solid state): 2058, 2044 (ν_{C=O}) cm⁻¹. Elemental analysis calcd (%) for C₂₈H₅₇NF₆O₂P₄Pd₃: C 33.7, N 1.41, H 5.76. Found: C 33.9, N 1.39, H 5.78.

4.11. Preparation of [Pd₃(μ-PBu₂)₃(CO)₂(NC₅H₅)]PF₆, (8)PF₆. An excess of TlPF₆ (32 mg, 0.094 mmol) was added to a red solution of **3** (44 mg, 0.047 mmol) in pyridine (3 mL) and the mixture was stirred for 3 days at room temperature. After this period the solvent was evaporated. The crude residue was washed with hexane and dissolved in acetone, and TlI was filtered off. Complex (8)PF₆ was obtained as a dark red solid (36 mg, 0.035 mmol, yield 74%) after evaporation of the solvent under vacuum. ¹H NMR (200 MHz, acetone-*d*₆, 293 K): δ = 8.21 (m, NC₅H₅, 2 H), 7.87 (m, NC₅H₅, 1 H), 7.63 (m, NC₅H₅, 2 H), 1.41 (d, ³J(H,P) = 15.0 Hz, CCH₃, 18 H), 1.29 ppm (vt, ³J(H,P) + ⁵J(H,P) = 7.4 Hz, CCH₃, 36 H). ¹³C{¹H} NMR (50.3 MHz, acetone-*d*₆, 293 K): δ = 186.2 (s, CO), 156.0 (s, NC₅H₅, 2 C), 140.2 (s, NC₅H₅, 1 C), 127.6 (s, NC₅H₅, 2 C), 41.5, 41.3 (s, PC-CH₃), 33.8, 33.4 ppm (s, PC-CH₃). ³¹P{¹H} NMR (81.0 MHz, acetone-*d*₆, 293 K): δ = 258.9 (d, ²J(P,P) = 121 Hz, 2 P), 250.8 (t, ²J(P,P) = 121 Hz, 1 P), -137.1 ppm (hept, ¹J(P,F) = 702 Hz, PF₆, 1 P). IR (solid state): 2066 (ν_{C=O}) cm⁻¹. Elemental analysis calcd (%) for C₃₁H₅₉NF₆O₂P₄Pd₃: C 36.0, N 1.35, H 5.75. Found: C 35.7, N 1.36, H 5.73.

4.12. Synthesis of [Pd₃(μ-PBu₂)₃(CNBu^t)₃](PF₆)₂, 6(PF₆)₂. AgPF₆ (13.4 mg, 0.053 mmol) was added to a solution of (6)I (30 mg, 0.026 mmol) in 3 mL of CH₂Cl₂. The orange solution turned immediately to dark pink, and a dark solid (Ag⁰ and AgI) precipitated out. The precipitate was filtered off, and the solvent was evaporated under vacuum. The crude residue was then washed with diethyl ether (3 × 2 mL). 6(PF₆)₂ was obtained as a dark pink solid (31 mg, 0.024 mmol, yield 92%) after solvent evaporation. ¹H NMR (200 MHz, acetone-*d*₆, 293 K): δ = 16.00 ppm (bs, PCCH₃, 54 H). IR (CH₂Cl₂): 2188 (ν_{C≡N}) cm⁻¹. IR (solid state): 2193 (ν_{C≡N}) cm⁻¹.

4.13. X-ray Diffraction Studies. The X-ray diffraction experiments were carried out at room temperature (*T* = 293 K) by means of a Bruker P4 diffractometer for **2** and a Bruker Smart Breeze CCD diffractometer for 6(CF₃SO₃). Both instruments operate with graphite-monochromated Mo Kα radiation. The samples were glued at the end of glass capillaries, and the intensity data collections were carried out until 2θ maximum of about 53°. The intensities were corrected for Lorentz and polarization effects and for absorption by means of semiempirical ψ-scan method²⁴ for the first sample and multiscan method for the second.²⁵

The unit cell parameters and diffraction symmetry suggested that the crystal structures of **2** and the one of Pd₃(μ-PBu₂)₃(CO)₂Cl⁵ were isotopic. Thus the refinement was started from the coordinates of the heavy atoms found in the latter. The hydrogen atoms were placed in calculated positions and were left to "ride" on the connected carbon atoms. The more relevant reliability factors obtained at the end of the refinement are listed in Table 4. The structure solution of 6(CF₃SO₃) was obtained by the direct methods contained in SHELXS97.²⁶ The slightly inconsistent geometry and the abnormal thermal parameters denounced the presence of a significant disorder in the anionic portion of the structure. The anion was refined as a rigid group placed in two partially superimposed limit positions, with the total occupancy fixed to 1.0. The excessive elongation of thermal ellipsoids of some carbon atoms of the *tert*-butyl groups of the cation suggested that they also were disordered. The two *tert*-butyl groups with the more anisotropic thermal ellipsoids in the final stages of the refinement were then introduced in the model, split in two limit positions. Some soft restraints had to be introduced in the refinement in order to limit the anisotropy of displacement parameters.

Subsequent cycles of refinement were made with anisotropic thermal parameters for the heavy atoms not involved in the disorder and led to a nearly equal occupancy of the two limit positions of the anion. The final reliability factors of the refinement are listed in Table

Table 4. Experimental Data for the X-ray Diffraction Studies of $\text{Pd}_3(\text{PBUt}_2)_3(\text{CO})_2\text{Br}$ (2**) and $[\text{Pd}_3(\text{PBUt}_2)_3(\text{CNBu}^t)_3](\text{CF}_3\text{SO}_3)_2$, **6**(CF_3SO_3)**

	2	6 (CF_3SO_3)
empirical formula	$\text{C}_{26}\text{H}_{52}\text{BrO}_2\text{P}_3\text{Pd}_3$	$\text{C}_{40}\text{H}_{81}\text{F}_3\text{N}_3\text{O}_3\text{P}_3\text{SPd}_3$
formula weight	888.70	1153.25
crystal system	orthorhombic	monoclinic
space group	$Pnma$ (No. 62)	$P2_1/n$ (No. 14)
$a/\text{\AA}$	18.084(2)	9.7168(6)
$b/\text{\AA}$	17.808(2)	19.8254(12)
$c/\text{\AA}$	11.8374(14)	28.9139(17)
β/deg		92.257(2)
$U/\text{\AA}^3$	3812.1(8)	5565.6(6)
Z	4	4
$D_{\text{calc}}/\text{Mg}\cdot\text{m}^{-3}$	1.548	1.376
μ/mm^{-1}	2.592	1.126
no. measured	5080	42271
no. unique $[R_{\text{int}}]$	4090 [0.0458]	10556 [0.0371]
no. of parameters	170	479
$R1, wR2$ [$I > 2\sigma(I)$] ^a	0.0565, 0.0979	0.0516, 0.1286
$R1, wR2$ [all data] ^a	0.1277, 0.1205	0.0788, 0.1465
goodness of fit ^a on F^2	0.988	1.026

^a $R(F_o) = \sum |F_o| - |F_c| / \sum |F_o|$; $R_w(F_o^2) = [\sum [w(F_o^2 - F_c^2)^2] / \sum [w(F_o^2)^2]]^{1/2}$; $w = 1/[\sigma^2(F_o^2) + (AQ)^2 + BQ]$ where $Q = [\text{MAX}(F_o^2, 0) + 2F_c^2]/3$; $\text{GOF} = [\sum [w(F_o^2 - F_c^2)^2] / (N - P)]^{1/2}$, where N and P are the numbers of observations and parameters, respectively.

4. In addition to the aforementioned software, other control calculations and preparation of publication material were performed with the programs contained in the suite WINGX.²⁷

■ ASSOCIATED CONTENT

Supporting Information

CIF files for compounds **2** and **6**(CF_3SO_3). This material is available free of charge via the Internet at <http://pubs.acs.org>.

■ AUTHOR INFORMATION

Corresponding Author

*E-mail: leoni@dcci.unipi.it.

Notes

The authors declare no competing financial interest.

■ ACKNOWLEDGMENTS

This work was supported by the Ministero dell'Istruzione, Università e Ricerca (MIUR), Project PRIN2008 No. 2008RFE3X, and by the Fondazione Cassa di Risparmio di Pisa under the "POLOPTEL" project no. 167/09.

■ REFERENCES

- (1) (a) Bender, R.; Braunstein, P.; Dedieu, A.; Ellis, P. D.; Huggins, B.; Harvey, P. D.; Sappa, E.; Tiripicchio, A. *Inorg. Chem.* **1996**, *35*, 1223–1234. (b) Itazaki, M.; Nishihara, Y.; Osakada, K. *Organometallics* **2004**, *23*, 1610–1621. (c) Itazaki, M.; Kitami, O.; Tanabe, M.; Nishihara, Y.; Osakada, K. *J. Organomet. Chem.* **2005**, *690*, 3957–3962. (d) Bender, R.; Braunstein, P.; Bouaoud, S.-E.; Merabet, N.; Rouag, D.; Zanello, P.; Fontani, M. *New J. Chem.* **1999**, *23*, 1045–1047. (e) Taylor, N. J.; Chieh, P. C.; Carty, A. J. *Chem. Commun.* **1975**, 448–449.
- (2) (a) Leoni, P.; Marchetti, F.; Pasquali, M.; Marchetti, L.; Albinati, A. *Organometallics* **2002**, *21*, 2176–2182. (b) Cavazza, C.; Fabrizi de Biani, F.; Funaioli, T.; Leoni, P.; Marchetti, F.; Marchetti, L.; Zanello, P. *Inorg. Chem.* **2009**, *48*, 1385–1397. (c) Leoni, P.; Manetti, S.;

Pasquali, M.; Albinati, A. *Inorg. Chem.* **1996**, *35*, 6045–6052. (d) Fabrizi de Biani, F.; Manca, G.; Marchetti, L.; Leoni, P.; Bruzzzone, S.; Guidotti, C.; Atrei, A.; Albinati, A.; Rizzato, S. *Inorg. Chem.* **2009**, *48*, 10126–10137.

(3) (a) Fabrizi de Biani, F.; Ienco, A.; Laschi, F.; Leoni, P.; Marchetti, F.; Marchetti, L.; Mealli, C.; Zanello, P. *J. Am. Chem. Soc.* **2005**, *127*, 3076–3089. (b) Leoni, P.; Marchetti, F.; Marchetti, L.; Pasquali, M.; Quagliarini, S. *Angew. Chem., Int. Ed.* **2001**, *40*, 3617–3618.

(4) (a) Albinati, A.; Leoni, P.; Marchetti, L.; Rizzato, S. *Angew. Chem., Int. Ed.* **2003**, *42*, 5990–5993. (b) Leoni, P.; Marchetti, F.; Marchetti, L.; Pasquali, M. *Chem. Commun.* **2003**, 2372–2373. (c) Albinati, A.; Balzano, F.; Fabrizi de Biani, F.; Leoni, P.; Manca, G.; Marchetti, L.; Rizzato, S.; Uccello-Barretta, G.; Zanello, P. *Inorg. Chem.* **2010**, *49*, 3714–3720.

(5) Arif, A. M.; Heaton, D. E.; Jones, R. A.; Nunn, C. M. *Inorg. Chem.* **1987**, *26*, 4228–4231.

(6) Dyer, P. W.; Fawcett, J.; Hanton, M. J.; Mingos, D. M. P.; Williamson, A.-M. *Dalton Trans.* **2004**, 2400–2401.

(7) Dell'Anna, M. M.; Mastroianni, P.; Nobile, C. F.; Calmuschi-Cula, B.; Englert, U.; Peruzzini, M. *Dalton Trans.* **2008**, 6005–6013.

(8) Reetz, M. T.; Bohres, E.; Goddard, R.; Holthausen, M. C.; Thiel, W. *Chem.—Eur. J.* **1999**, *5*, 2101–2108.

(9) Leoni, P.; Sommovigo, M.; Pasquali, M.; Sabatino, P.; Braga, D. J. *Organomet. Chem.* **1992**, *423*, 263–270.

(10) Arifhodzic-Radojevic, S.; Burrows, A. D.; Choi, N.; McPartlin, M.; Mingos, D. M. P.; Tarlton, S. V.; Vilar, R. *J. Chem. Soc., Dalton Trans.* **1999**, 3981–3988.

(11) Leoni, P.; Vichi, E.; Lencioni, S.; Pasquali, M.; Chiarentin, E.; Albinati, A. *Organometallics* **2000**, *19*, 3062–3068.

(12) (a) Bonaccorsi, C.; Fabrizi de Biani, F.; Leoni, P.; Marchetti, F.; Marchetti, L.; Zanello, P. *Chem.—Eur. J.* **2008**, *14*, 847–856. (b) Leoni, P.; Pasquali, M.; Fortunelli, A.; Germano, G.; Albinati, A. *J. Am. Chem. Soc.* **1998**, *120*, 9564–9573. (c) Leoni, P.; Marchetti, F.; Pasquali, M.; Marchetti, L.; Albinati, A. *Organometallics* **2002**, *21*, 2176–2182. (d) Leoni, P.; Marchetti, F.; Paoletti, M. *Organometallics* **1997**, *16*, 2146–2151.

(13) Scott, D.; Pregosin, P. S.; Veiros, L. F.; Calhorda, M. J. *Organometallics* **2005**, *24*, 5710–5717.

(14) (a) The CSD System. The Cambridge Structural Database: A quarter of a million crystal structures and rising; Allen, F. H. *Acta Crystallogr.* **2002**, *B58*, 380–388. (b) ConQuest: New software for searching the Cambridge Structural Database and visualizing crystal structures; Bruno, I. J.; Cole, J. C.; Edgington, P. R.; Kessler, M.; Macrae, C. F.; McCabe, P.; Pearson, J.; Taylor, R. *Acta Crystallogr.* **2002**, *B58*, 389–397.

(15) Mealli, C. *J. Am. Chem. Soc.* **1985**, *107*, 2245–2253.

(16) (a) Geiger, W. E.; Barriere, F. *Acc. Chem. Res.* **2010**, *43*, 1030–1039. (b) Evans, D. H. *Chem. Rev.* **2008**, *108*, 2113–2144.

(17) (a) Janzen, D. E.; vanDeerver, D. G.; Mehne, L. F.; da Silva Filho, D. A.; Bredas, J.-L.; Grant, G. J. *Dalton Trans.* **2008**, 1872–1882. (b) Dey, S.; Jain, V. K.; Knödler, A.; Klein, A.; Kaim, W.; Zalis, S. *Inorg. Chem.* **2002**, *41*, 2864–2870. (c) Evrard, D.; Clement, S.; Lucas, D.; Hanquet, B.; Knorr, M.; Strohmman, C.; Decken, A.; Mugnier, Y.; Harvey, P. D. *Inorg. Chem.* **2006**, *45*, 1305–1315. (d) Roy, S.; Hartenbach, I.; Sarkar, B. *Eur. J. Inorg. Chem.* **2009**, 2553–2558. (e) Kamath, S. S.; Uma, V.; Srivastava, T. S. *Inorg. Chim. Acta* **1989**, *161*, 49–56. (f) Smucker, B. W.; Hudson, J. M.; Omart, M. A.; Dunbar, K. R. *Inorg. Chem.* **2003**, *42*, 4714–4723. (g) Waggoner, N. W.; Spreer, L. S.; Boro, B. J.; DuBois, D. L.; Helm, M. L. *Inorg. Chim. Acta* **2012**, *380*, 14–21. (h) Matsumoto, K.; Takahashi, K.; Ikuzawa, M.; Kimoto, H.; Okeya, S. *Inorg. Chim. Acta* **1998**, *281*, 174–180. (i) Shin, K.-S.; Son, K.-I.; Kim, J. I.; Hong, C. S.; Suh, M.; Noh, D.-Y. *Dalton Trans.* **2009**, 1767–1775. (j) Cai, X.; Donzello, M. P.; Viola, E.; Rizzoli, C.; Ercolani, C.; Kadish, K. M. *Inorg. Chem.* **2009**, *48*, 7086–7098. (k) Bulak, E.; Leboschke, M.; Schwederski, B.; Sarper, O.; Varnali, T.; Fiedler, J.; Lissner, F.; Schleid, T.; Kaim, W. *Inorg. Chem.* **2007**, *46*, 5562–5566.

(18) (a) When the electron transfer processes involve orbitals that are mainly ligand centered, the shift may be occasionally^{18b-d} reversed

$[E^\circ_n(\text{Pd}) - E^\circ_n(\text{Pt}) < 0]$. (b) Pugliese, T.; Godbert, N.; Aiello, I.; La Deda, M.; Ghedini, M.; Amati, M.; Belvisio, S.; Lelij, F. *Dalton Trans.* **2008**, 6563–6572. (c) Sun, X.; Chun, H.; Hildenbrand, K.; Bothe, E.; Weyhermüller, T.; Neese, F.; Wieghardt, K. *Inorg. Chem.* **2002**, *41*, 4295–4303. (d) Matas, I.; Whittell, G. R.; Partridge, B. M.; Holland, J. P. M.; Haddow, F.; Green, J. C.; Manners, I. *J. Am. Chem. Soc.* **2010**, *132*, 13279–13289.

(19) (a) Dal Molin, S.; Mugnier, Y.; Fortin, D.; Harvey, P. D. *Dalton Trans.* **2010**, 39, 8976–8981. (b) Brevet, D.; Lucas, D.; Mugnier, Y.; Harvey, P. J. *Cluster Sci.* **2006**, *17*, 5–12.

(20) Funaioli, T.; Leoni, P.; Marchetti, L.; Albinati, A.; Rizzato, S.; Fabrizi de Biani, F.; Ienco, A.; Manca, G.; Mealli, C. *Inorg. Chem.* **2013**, *52*, 4635–4647.

(21) The oxidation of I^- in $[\text{Bu}_4\text{N}]\text{I}/\text{CH}_2\text{Cl}_2$ solution is superimposed to that of **3**; this causes the consumption of an amount of charge larger than expected during the electrolysis. Moreover, it is worth noting that the reversible wave at -0.27 was observed also when **3** was electrolyzed in the absence of $[\text{Bu}_4\text{N}]\text{I}$ (see the beginning of section 2.4.1), in which conditions the reversible reduction at -0.88 V was masked by more intense irreversible reduction waves.

(22) King, R. B.; Bisnette, M. B. *J. Organomet. Chem.* **1967**, *8*, 287–297.

(23) Krejčík, M.; Daněk, M.; Hartl, F. J. *Electroanal. Chem.* **1991**, *317*, 179–187.

(24) XPREP—Program for data reduction; Bruker-AXS Inc.: Madison, WI, 1998.

(25) Sheldrick, G. M. *SADABS, Program for empirical absorption correction*; University of Göttingen: Göttingen, Germany, 1996.

(26) Sheldrick, G. M. *SHELX97, Programs for Crystal Structure Analysis (Release 97-2)*; University of Göttingen: Göttingen, Germany, 1998.

(27) Farrugia, L. J. *J. Appl. Crystallogr.* **1999**, *32*, 837–838.